I&EC research
Industrial & Engineering Chemistry Research

pubs.acs.org/IECR

Article

Demethylation of Waste Alkali Lignin for Rapid and Efficient Ammonia Adsorption

Jian-Fei Li, Zhang-Min Li,* Jian-Bo Xu, Cheng-Yong Guo, Guo-Wen Fang, Yan Zhou, Ming-Shuai Sun, and Duan-Jian Tao*

Cite This: *Ind. Eng. Chem. Res.* 2024, 63, 3282−3289

Read Online

ACCESS | Metrics & More | Article Recommendations | Supporting Information

ABSTRACT: Alkali lignin, a significant waste resource from the pulp and paper industry, is produced in large quantities each year, but its utilization remains limited. This study focuses on the cleavage of $-OCH_3$ groups attached to the aromatic ring in alkali lignin to obtain demethylated alkali lignin nanospheres (DAL-NPs) enriched with aromatic hydroxyl (Ar−OH) groups. These DAL-NPs are intended for the efficient adsorption of NH_3. Qualitative and quantitative characterization of alkali lignin, both pre- and post-demethylation, was performed using Fourier transform infrared spectroscopy and ^1H NMR. The analysis revealed a reduction in methoxy groups and an increase in Ar−OH groups in the DAL-NPs. The NH_3 adsorption experiment demonstrated that the DAL-NPs exhibited a rapid and high adsorption capacity, reaching an NH_3 uptake capacity of 10.0 mmol g^{-1} within 0.42 min at 298 K and 1.0 bar. In addition, the DAL-NPs displayed superior selectivity based on the ideal adsorption solution theory for 10% NH_3/90% N_2 (3252) and 10% NH_3/90% CO_2 (175) at 298 K and 1.0 bar. The DAL-NPs also demonstrated reversibility and stability during 10 adsorption−desorption cycles. The DAL-NP adsorbent possesses exceptional properties, such as abundance and low cost, rapid and efficient adsorption, reversibility, and stability, making it a promising solid adsorbent for effective NH_3 adsorption in the ammonia process.

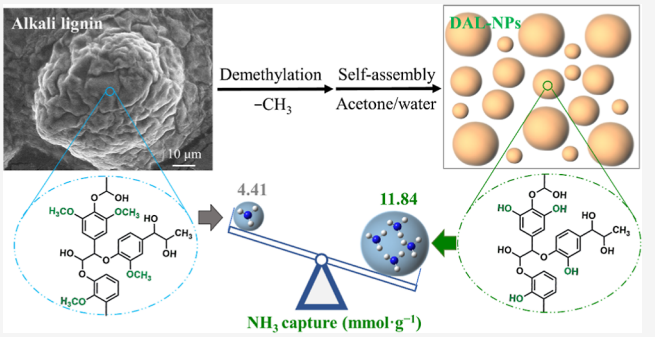

1. INTRODUCTION

Alkali lignin, the primary component derived from the soda pulp industry, accounts for over 85% of the world's industrial lignin generation, with an annual yield of 40−50 million tons.[1,2] Despite its significant production volume, alkali lignin remains severely underutilized in current practices due to its recalcitrant and complex structure. As a result, it is often disposed of as wastewater or incinerated without reuse. This leads to significant resource wastage and contributes to environmental issues, such as river pollution and high greenhouse gas emissions.[3,4] Therefore, it is essential to explore strategies for modifying alkali lignin by equipping it with specific functional groups to enable practical applications. For instance, alkali lignin can be tailored into functional polymers capable of removing heavy metal ions and dyes,[5−9] or it can be employed as dispersants.[10,11] Additionally, it shows potential for developing lignin-based nanomaterials through physical or chemical methods.[12,13]

Ammonia (NH_3) is a crucial substance in the chemical industry, serving as a feedstock in the manufacture of nitrogen fertilizers, nitrous oxide, alternative fuels, plastics, and dyes.[14,15] However, NH_3 is also a corrosive air contaminant, posing significant challenges. When released into the atmosphere, NH_3 reacts with NO_X and SO_X, resulting in the formation of secondary pollutants such as NH_4NO_3 and $(NH_4)_2SO_4$. These compounds contribute to the generation of PM 2.5 and acid rain, which can cause significant harm to both human health and the environment.[16−19] With an estimated global annual production of almost 200 million tons of NH_3, the widespread use of this compound increases the risk of potential leakage during production processes.[20,21] Therefore, there is an urgent need to remove NH_3 from air and control its concentration to levels that are relatively safe.

Adsorption is widely recognized as a favorable method for the economic and efficient removal of low concentrations of NH_3 from industrial emissions.[22] The choice of the adsorbent plays a critical role in the process. Various adsorbent materials, including carbon-based adsorbents,[23−26] alumina,[27] silica,[18,28] and metal-organic frameworks (MOFs),[17,19,29−32] have been developed and modified to functionalized surfaces and porous structures, allowing for effective removal of NH_3. For instance,

Received: December 5, 2023
Revised: February 1, 2024
Accepted: February 5, 2024
Published: February 12, 2024

https://doi.org/10.1021/acs.iecr.3c04306
Ind. Eng. Chem. Res. 2024, 63, 3282−3289

Scheme 1. Schematic of the Production of Ar−OH-Rich Lignin by Alkali Lignin Demethylation

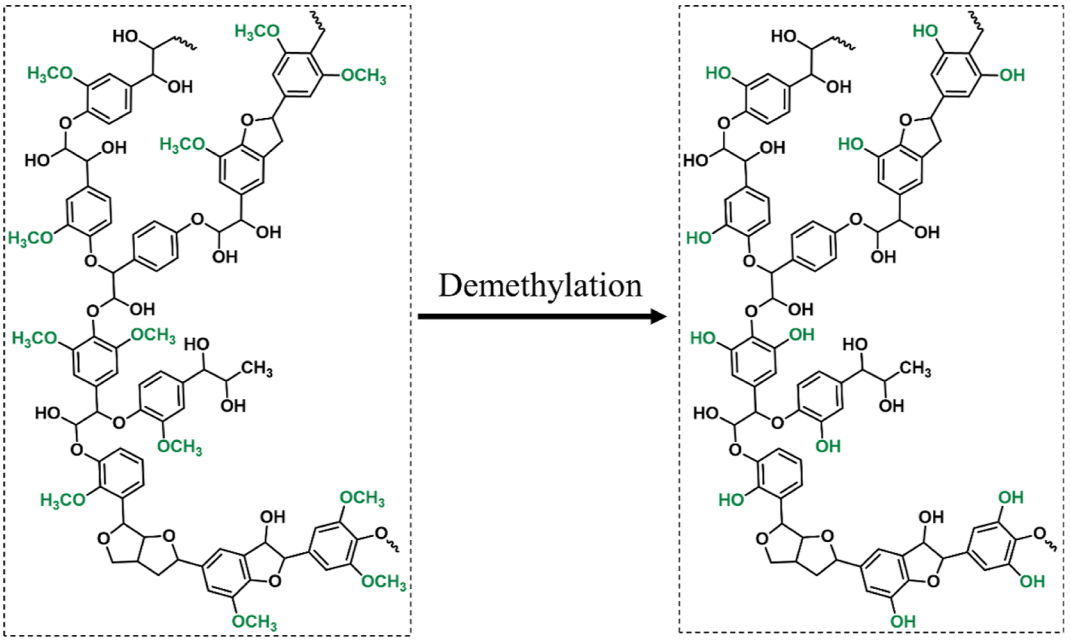

Wang et al.[29] used the MOF MIL-53-$(OH)_2$ as a base material and incorporated lithium chloride within its nanopore channels to achieve high-performance heterogeneous MOF adsorbents for NH_3 capture. Although these adsorbents have demonstrated favorable adsorption outcomes, they exhibit certain drawbacks such as complexity, high cost, low yield of prepared adsorbents, and limited separation selectivity, making them less suitable for industrial applications.[27] Our research group has recently synthesized three sulfonated phenol-formaldehyde resins that feature aromatic hydroxyl (Ar−OH) and sulfonate groups as acid sites to facilitate NH_3 adsorption.[33] Alkali lignin, which consists of H, G, and S units, contains a substantial amount of methoxy and hydroxyl groups attached to aromatic rings.[34,35] By removing the methyl group from the methoxy group attached to the lignin's aromatic ring, an adsorbent material rich in weakly acidic Ar−OH sites can be obtained.[36,37] This material has tremendous potential as an efficient adsorbent for capturing alkaline NH_3.

Herein, the focus of this study is the demethylation of alkali lignin to produce Ar−OH-rich lignin (Scheme 1). The resulting demethylated alkali lignin nanospheres (DAL-NPs) are then used as adsorbents for the separation and capture of NH_3. To obtain the variation of the lignin demethylation efficiency and Ar−OH content, alkali lignin before and after demethylation was characterized by Fourier transform infrared (FT-IR) spectroscopy and quantitative ^{1}H NMR. Then, the adsorption performance of DAL-NPs on NH_3 was systematically investigated, including adsorption capacity and separation selectivity. In addition, to explore their potential industrial applications, their recyclability and breakthrough performance in a $NH_3/N_2/CO_2$ mixture were also investigated.

2. MATERIALS AND METHODS

2.1. Materials. Lithium bromide (99%) and hydrogen bromide (48% by weight) were procured from Shanghai Adamas Reagent Co. Ltd. Alkali lignin and γ-valerolactone (98%) were supplied by Shanghai Maclean Biochemical Technology Co. High-purity N_2 (99.999%), NH_3 (99.999%), and CO_2 (99.999%) were sourced from Jiangxi Huahong Special Gas Co. The experimental procedures utilized all solvents directly. The deionized water used in this study was prepared in-house in the laboratory.

2.2. Preparation of Demethylated Alkali Lignin Nanoparticles. The method for preparing demethylated alkali lignin nanoparticles (DAL-NPs) has been refined based on previously reported methods.[38,39] In a typical procedure, a hydrothermal reactor was charged with 6.1 g of lithium bromide and 3.9 g of water. The mixture was stirred for 2 min until the lithium bromide was completely dissolved, resulting in a colorless solution. 0.5 g of alkali lignin and 1.0 mL of HBr (1.48 g, 48 wt %) were added to the solution. The reaction mixture was heated and maintained at 373 K for 4 h. After completion, the hydrothermal reactor was cooled, and the solid residue at the bottom was collected by centrifugation. It was then washed three times until the pH of the supernatant reached neutrality. The solid sample was solubilized in a solvent mixture of γ-valerolactone and water (4:1, v/v) with a mass (mg)/volume (mL) ratio of 40:1. Subsequently, 1.0 mL of the resulting lignin solution was slowly added dropwise to 50 mL of deionized water, gently stirred at 303 K for 2 h, and centrifuged at 8500 rpm for 12 min. The resulting brownish solid was washed three times with fresh deionized water and subjected to lyophilization, ultimately yielding DAL-NPs.

2.3. Characterization Methods. The detailed characterization techniques and procedures are given in the Supporting Information. The ^{1}H NMR characterization of lignin samples underwent an acetylation reaction following demethylation to enhance the solubility of lignin in the deuterium solvent (DMSO-d_6) and enable accurate analysis.[40]

2.4. NH_3 Adsorption Procedure. The isotherms of NH_3 capture were investigated at different temperatures and pressures by using a two-chamber volumetric method developed in-house. Further details can be found in the Supporting Information (Figures S1 and S2). The experimental setup involved monitoring of the uptake process with a

https://doi.org/10.1021/acs.iecr.3c04306
Ind. Eng. Chem. Res. 2024, 63, 3282−3289

digital indicator (NI). Gas adsorption used approximately 0.1 g of the adsorbent.

3. RESULTS AND DISCUSSION

3.1. Characterization of Lignin. Figure 1 shows the FT-IR spectra of alkali lignin and DAL-NPs. The spectrum showed

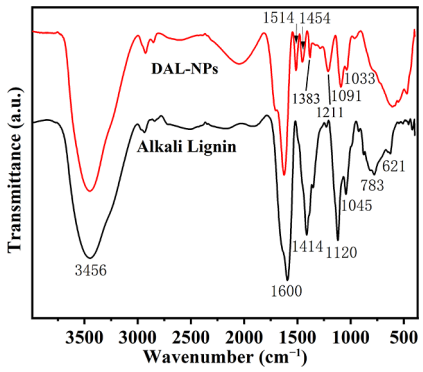

Figure 1. FT-IR spectra of alkali lignin and DAL-NPs.

a broad signal absorbance at 3456 cm^{-1}, which is indicative of the presence of O−H stretching in alcoholic and phenolic hydroxyl groups.[41] The spectra display distinct peaks corresponding to the aromatic ring C═C bonds at 1450−1600 cm^{-1} and the C−H bonds in the region of 700−850 cm^{-1}.[42] The peaks observed at 1045 and 1120 cm^{-1} are mainly due to the stretching of the C−H bonds of the $-OCH_3$ group. The peak at 1414 cm^{-1} may be attributed to sodium hydroxide residues present in alkali lignin or the aromatic ring itself. Upon analysis of the demethylated alkali lignin nanoparticles in comparison to the alkali lignin, a significant reduction in the characteristic peaks related to sodium hydroxide (1414 and 783 cm^{-1}) was observed. This suggests that the demethylation process effectively eliminates sodium hydroxide impurities. Upon removal of sodium hydroxide, two previously obscured peaks (1514 and 1454 cm^{-1}) became visible. These peaks correspond to the C−C and C═C stretching vibrations of the lignin aromatic skeleton and the C−O stretching vibration peak of the benzene ring linking the methoxy Ar−OCH_3.[42,43] Additionally, the FT-IR spectra show a notable reduction in the $-OCH_3$ peak (1045 and 1120 cm^{-1}) of DAL-NPs, while the peak corresponding to the Ar−OH group at 1211 cm^{-1} was increased.[44] These results suggest that demethylation decreases the quantity of $-OCH_3$ groups and enhances the characteristic peaks associated with Ar−OH groups in the DAL-NPs material.

To identify functional groups containing hydrogen, we quantified lignin before and after demethylation using ^1H NMR spectroscopy. Figure 2 shows the proton signals observed during the analysis. The signal at 10.16 ppm was assigned to CHO groups, and signals at 8.47 and 8.16 ppm were allocated to the aromatic protons of the internal standard of *p*-nitrobenzaldehyde (NBA). The proton signal observed at 3.75 ppm corresponds to the $-OCH_3$ group in lignin. The two peaks at 2.26 and 2.00 ppm were identified as the aromatic and aliphatic superacetyl groups of lignin, respectively. Protons of the aliphatic portion of lignin were observed in the range of 0.8−1.5 ppm. The analysis indicates that after the demethylation reactions, some Ph−OCH_3 groups are converted into Ar−OH groups.

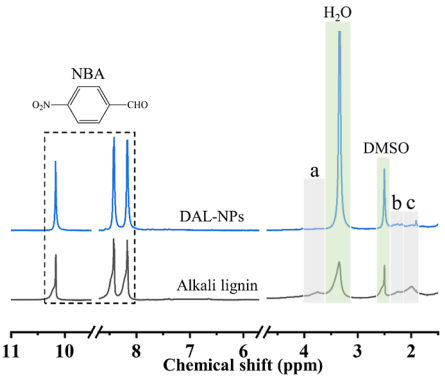

Figure 2. ^1H NMR spectrum of alkali lignin and DAL-NPs (a corresponds to the $-OCH_3$ group and parts b and c correspond to the aromatic and aliphatic acetyls, respectively).

The mass fraction of the $-OCH_3$ or Ar−OH group of lignin was determined by analyzing the ^1H NMR spectrum with NBA as an internal reference with a characteristic peak at 10.2 ppm. The results are presented in Table 1. Compared to that of alkali lignin, the content of $-OCH_3$ in DAL-NPs decreased from 1.38 to 0.59 mmol g^{-1}, whereas the Ar−OH content increased from 0.52 to 0.84 mmol g^{-1}.

Figure S3 shows that alkali lignin contains significant amounts of Na elements along with C and O elements. However, DAL-NPs do not contain any Na elements. This observation is consistent with the FT-IR characterization results, which suggest that the demethylation process effectively removes sodium hydroxide impurities from the alkali lignin through acid and water washing.

Scanning electron microscopy (SEM) was used to characterize the surface morphologies of alkali lignin and DAL-NPs. Figure 3c,d shows that the initial alkali lignin has larger clusters or aggregates, while DAL-NPs exhibit well-defined nanospheres. The nanospherical shape facilitates the diffusion and adsorption of gas molecules.

Figure 4 shows additional sorption isotherms of alkali lignin and DAL-NPs conducted under a nitrogen atmosphere. The results demonstrate that the isotherms of alkali lignin exhibit a significantly lower N_2 adsorption capacity, as well as a limited surface area of 0.95 m^2 g^{-1}. Notably, N_2 adsorption occurs primarily at 0.9−1.0P/P_0, indicating the existence of slit pores within the sample.

Thermogravimetry (TG) analysis was performed on alkali lignin and DAL-NPs to examine their thermal behavior, as shown in Figure S4. The analysis indicated a 5% thermogravimetric loss for both lignins and DAL-NPs when the temperature was increased from 303 to 373 K, mainly due to the removal of free water. Subsequently, as the temperature increased, the samples entered the thermal decomposition phase; during this phase, chemical bonds, mainly C−O and C−C bonds, were broken, resulting in the generation of volatiles. At 773 K, both samples completely decomposed, leaving behind coke residues. The final coke residue percentages were determined to be 36.64% for alkali lignin and 46.14% for DAL-NPs. The TG analysis indicates that both materials are stable at temperatures below 373 K.

3.2. NH_3 Uptake Performance. Figure 5a shows the NH_3 uptake rates of alkali lignin and DAL-NPs at 298 K and 1 bar. Both alkali lignin and DAL-NPs exhibited rapid adsorption rates for NH_3, reaching equilibrium within 2.5 min. The NH_3 uptake capacity of 10.0 mmol g^{-1} was achieved within 0.42

https://doi.org/10.1021/acs.iecr.3c04306
Ind. Eng. Chem. Res. 2024, 63, 3282−3289

Table 1. Chemical Shifts and Relative Proportions of $-OCH_3$ and Ar−OH Groups in Alkali Lignin and DAL-NPs[a]

lignin sample	M (mg)	M_i (mg)	chemical shift (ppm)			F_{Ar-OH} (mmol g^{-1})	F_{MeO} (mmol g^{-1})
			I_i δ10.4−10.2	I_{Ar-OH} δ2.5−2.17	I_{MeO} δ4.0−3.48		
alkali lignin	20	5	2	4.16	11.04	0.52	1.38
DAL-NPs	20	5	2	6.72	4.72	0.84	0.59

[a]M represents the weight of alkali lignin or DAL-NPs (mg), M_i represents the weight of NBA (mg), I_i represents the peak area of NBA, and F represents the specific content of certain groups (mmol g^{-1}).

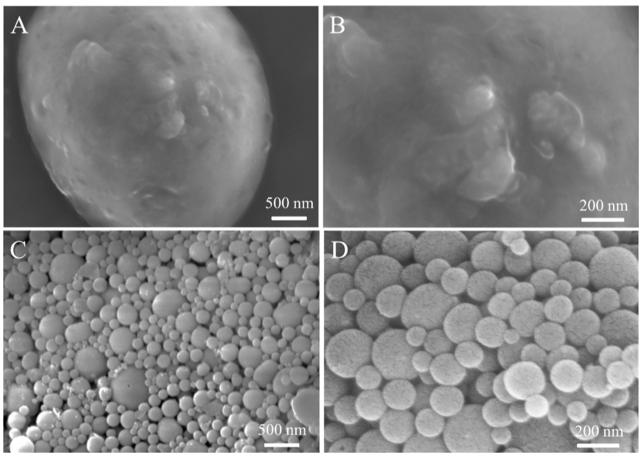

Figure 3. SEM images of alkali lignin (A,B) and DAL-NPs (C,D).

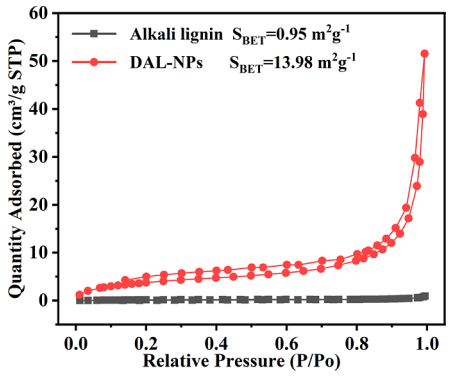

Figure 4. N_2 sorption isotherms of alkali lignin and DAL-NPs.

min at 298 K and 1.0 bar. DAL-NPs had a higher NH_3 uptake capacity (11.84 mmol g^{-1}) than alkali lignin (4.41 mmol g^{-1}) under the same conditions. This observation suggests that DAL-NPs have a higher concentration of acidic Ar−OH groups than alkali lignin, which enhances their NH_3 sorption capacity. Additionally, we conducted experiments to examine the adsorption rate of DAL-NPs at different temperatures (Figure 5a). Surprisingly, it is found that temperature did not have a significant impact on the equilibrium time (~2.5 min) for NH_3 adsorption by DAL-NPs. However, the adsorption capacity is significantly affected by the temperature, indicating a significant decrease in adsorption capacity with increasing temperature. Similar results have been reported in the relevant literature.[33,45−47]

To investigate the impact of the pressure on NH_3 adsorption by DAL-NPs, we conducted static adsorption experiments to measure the adsorption isotherms of DAL-NPs at various pressures. Figure 5b shows an increase in the NH_3 gas adsorption capacity of DAL-NPs with increasing pressure, indicating that NH_3 adsorption by DAL-NPs becomes more favorable under higher pressure conditions. The isothermal heat of the reaction was determined to be within the range of −30 to −25 kJ mol^{-1} by establishing the relationship among NH_3 uptake, capacity, and temperature (see Figure S5).

In the ammonia industry, flue gases commonly contain a mixture of NH_3, N_2, and CO_2. Therefore, it is important to assess the selectivity of DAL-NPs in separating NH_3 from gas mixtures. Figure 5c shows the adsorption capacity of DAL-NPs for NH_3, N_2, and CO_2 at various pressures and at a temperature of 298 K. It is clear that the uptake capacity of DAL-NPs for N_2 and CO_2 is significantly lower than that for NH_3 at different pressures. Furthermore, we conducted additional investigations into the IAST selectivities for NH_3/CO_2 and NH_3/N_2 at varying NH_3 molar fractions (Figure 5d). The results demonstrate that DAL-NPs exhibit exceptional selectivity for separating NH_3/N_2 and NH_3/CO_2 mixtures, with IAST selectivity values of 3252 for NH_3/N_2 (10/90, v/v) and 175 for NH_3/CO_2 (10/90, v/v). These findings highlight the significant potential of DAL-NPs as an excellent adsorbent for NH_3 capture.

3.3. Breakthrough Performance of DAL-NPs. To evaluate the practical performance of DAL-NPs in separating NH_3/CO_2 and NH_3/N_2 under real conditions, we studied a flue gas mixture consisting of 96% N_2, 1% CO_2, and 3% NH_3. We examined the breakthrough behavior of DAL-NPs was examined at 303 K and 1 bar, with a gas streamflow rate of 20.0 mL min^{-1}. Figure 6a shows a gradual breakthrough of NH_3 on DAL-NPs, with a residence time of approximately 100 min g^{-1}. These results demonstrate that DAL-NPs can effectively and selectively eliminate NH_3, even in the presence of N_2 and CO_2. This highlights the potential of DAL-NPs for use in the fuel gas treatment.

3.4. Regeneration Performance. To investigate the cycling stability of DAL-NPs, we subjected the sample that had reached adsorption saturation to a vacuum desorption process at 353 K and 0.1 kPa for 2.5 h, resulting in the recovery of the desorbed DAL-NPs. We subsequently measured the adsorption capacity of DAL-NPs for NH_3 again and repeated the process 10 times to assess the cycling performance. Figure 6b shows that there was no discernible change in the adsorption capacity of DAL-NPs for NH_3 after 10 cycles. Furthermore, the FT-IR spectra of the cyclically desorbed DAL-NPs are shown in Figure S6. A prominent peak at 1393 cm^{-1} is observed, which is due to the formation of NH_4^+ resulting from the interaction between NH_3 and Ar−OH in DAL-NPs.[18] Additionally, no significant changes in characteristic peaks were observed in the FT-IR spectra of the cyclically desorbed DAL-NPs when compared to those of the fresh DAL-NPs. Table S1 displays the elemental composition of the DAL-NPs adsorbent before and after NH_3 desorption. The results demonstrate that the content of elemental N remains stable without significant changes, and the content of other elements (C, H, and O) is also consistent. Therefore, it can be concluded that the DAL-NP material is capable of completely

https://doi.org/10.1021/acs.iecr.3c04306
Ind. Eng. Chem. Res. 2024, 63, 3282−3289

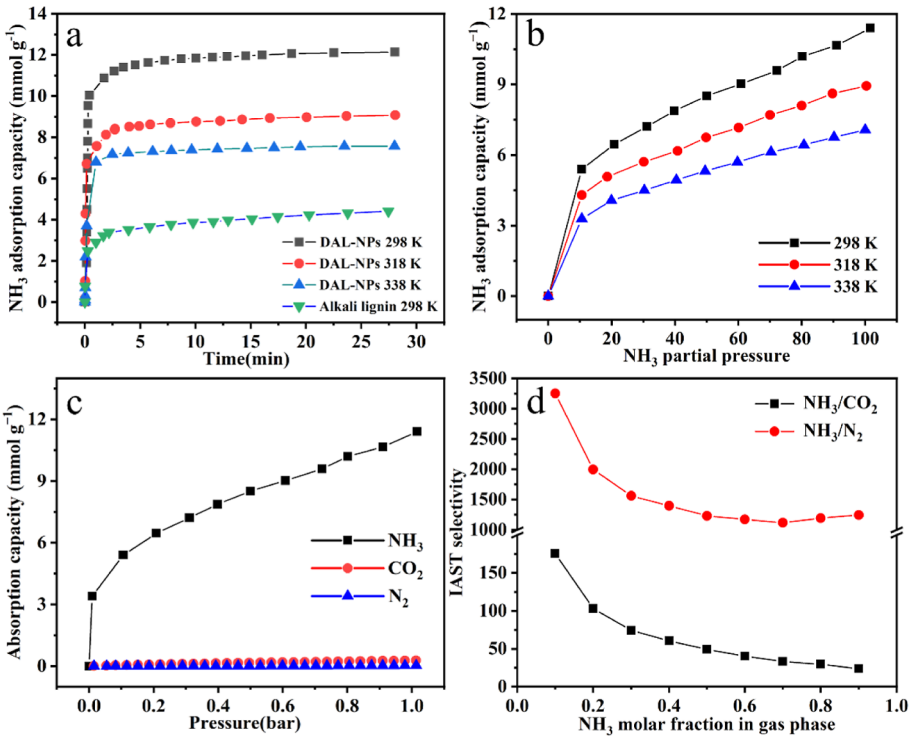

Figure 5. (a) NH_3 adsorption rate of alkali lignin and DAL-NPs, (b) influence of temperature on NH_3 adsorption through DAL-NPs, (c) NH_3, CO_2, and N_2 uptake isotherms of DAL-NPs at 298 K, 1 bar, and (d) IAST selectivities to NH_3/CO_2 and NH_3/N_2.

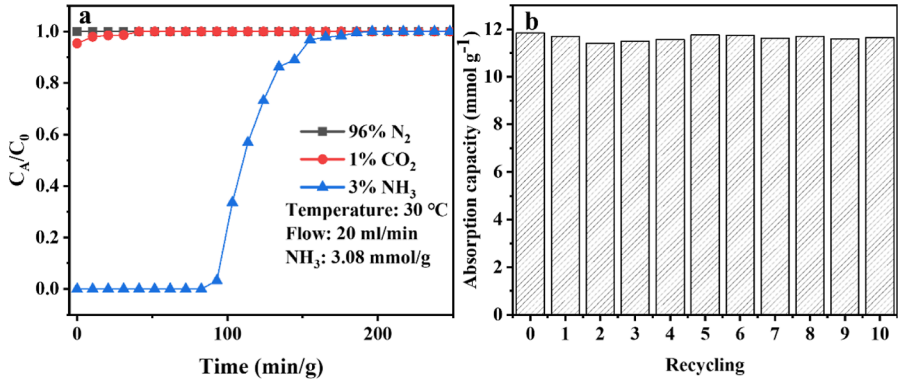

Figure 6. (a) Experimental breakthrough curves of simulated NH_3 flue gas separation by DAL-NPs at 303 K and (b) recycling performance of DAL-NPs for NH_3 adsorption and desorption at 298 K.

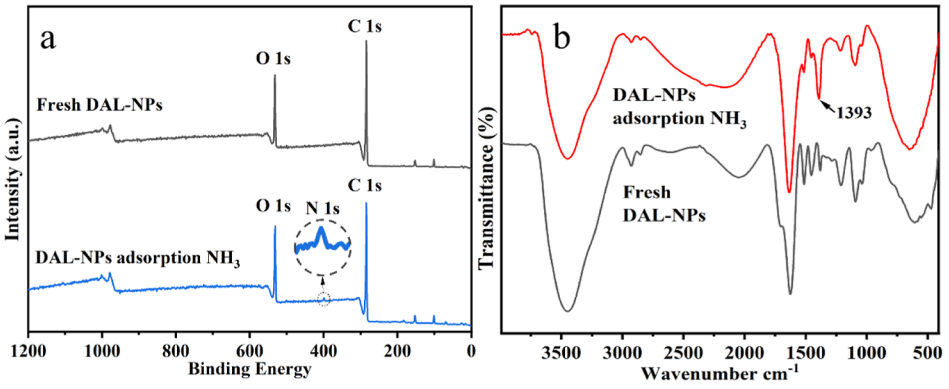

Figure 7. (a) XPS curves and (b) FT-IR images of fresh DAL-NPs and DAL-NPs adsorption of NH_3.

desorbing NH_3 while remaining stable. The finding is consistent with the FT-IR characterization presented in Figure S6, which shows that NH_3 can be efficiently desorbed from the Ar−OH-rich adsorbent, indicating exceptional recyclability.

https://doi.org/10.1021/acs.iecr.3c04306
Ind. Eng. Chem. Res. 2024, 63, 3282−3289

Table 2. NH_3 Adsorption Capacity and Recycling Performance of the Adsorbents and Other Adsorbents in the Literature

entry	absorbents	NH_3 capacity (mmol·g^{-1})		recycling conditions	NH_3 adsorption uptake loss	refs
		0.1 bar	1.0 bar			
1	alkali lignin	1.74	4.41			this work
2	DAL-NPs	5.40	11.84	353 K, 2 h	almost no less (10 cycles)	this work
3	organosolv lignin	2.10	5.45			this work
4	de-organosolv lignin	4.91	11.62	353 K, 2 h	almost no less (8 cycles)	this work
5	NU-300	4.05	8.28	393 K, 12 h	~35%(3 cycles)	48
6	PAA	5.73	10.70	353 K, 18 h	13% (5 cycles)	49
7	PI	4.21	9.00	353 K, 18 h	almost no less (5 cycles)	49
8	BIDC-2-700	6.24	14.26	298 K	~21% (2 cycles)	25
9	BIDC-0.5-750	3.84	11.47	298 K	~5% (2 cycles)	25
10	PIM-1-COOH	7.05	12.2	298 K	~11% (3 cycles)	50
11	CuC_2O_4/BGB-2-600-0.7	1.45	8.68	298 K, 2 h	~25% (8 cycles)	53
12	PDVB-2.0AA	4.51	8.83	353 K, 2 h	11.2% (10 cycles)	52

3.5. Mechanism of NH_3 Absorption. X-ray photoelectron spectroscopy (XPS) and FT-IR characterization of the materials before and after adsorption were conducted to investigate the adsorption mechanism of NH_3 by DAL-NPs (Figure 7). The wide XPS spectrum in Figure 7a shows a small peak at 399.7 eV in the adsorbent after NH_3 adsorption, which can be attributed to the peak of N 1s in adsorbed NH_3, compared to that of fresh DAL-NPs. In addition, the FT-IR analysis showed an extra peak at 1393 cm^{-1} (Figure 7d), which corresponds to the N−H stretching vibration after the adsorption of DAL-NPs. This indicates that DAL-NPs successfully adsorbed NH_3. The phenolic hydroxyl group on the surface of the DAL-NPs material is widely recognized to exhibit weak acidity. Therefore, the adsorption of NH_3 by DAL-NPs materials is achieved through the interaction between the phenolic hydroxyl group with weak acidity on the surface of DAL-NPs and alkaline NH_3, which results in efficient NH_3 capture.

3.6. Comparison of DAL-NPs with Other Adsorbents in the Literature. Table 2 compares DAL-NPs and organosolv lignin from bamboo with other published porous adsorbents, including NU-300,[48] PAA,[49] BIDC-2-700,[25] PIM-1-COOH,[50] CuC_2O_4/BGB-2-600-0.7,[51] and PDVB-2.0AA,[52] for their NH_3 adsorption capacity and cycling performance. The NH_3 capture performance of DAL-NPs is 2.7 times higher than that of alkali lignin (11.84 vs 4.41 mmol·g^{-1}) at 298 K and 1 bar. The NH_3 uptake capacity of DAL-NPs exceeds that of NU-300, PAA, PI, CuC_2O_4/BGB-2-600-0.7, and PDVB-2.0AA. Notably, NU-300, BIDC-2-700, and CuC_2O_4/BGB-2-600-0.7 exhibit significant reductions in NH_3 uptake capacity during recycling. For example, Table 2 shows that NU-300 experiences a loss of almost 35% after three cycles due to the high interaction between their adsorption sites and NH_3, with adsorption enthalpy exceeding −50 kJ·mol^{-1}.[33] This makes complete desorption of adsorbed NH_3 challenging. In contrast, DAL-NPs exhibit almost no loss of NH_3 uptake capacity even after 10 cycles and can be fully desorbed under mild conditions. Overall, the DAL-NP adsorbent demonstrates satisfactory NH_3 adsorption capacity, excellent reversibility, and high selectivity for adsorbing NH_3 in the $NH_3/CO_2/N_2$ mixture.

4. CONCLUSIONS

This work successfully demethylated a significant amount of alkali lignin from pulp and paper to produce DAL-NPs. The resulting DAL-NPs were characterized and found to possess a higher concentration of Ar−OH groups than that of alkali lignin. Efficient NH_3 adsorption is achieved using DAL-NPs as an adsorbent. The experimental results demonstrate a large NH_3 uptake capacity of 11.84 mmol g^{-1} and rapid attainment of adsorption equilibrium within 5 min. Furthermore, DAL-NPs demonstrate exceptional selectivity for separating NH_3/CO_2 and NH_3/N_2, as demonstrated by IAST selectivity values of 175 and 3252, respectively. The breakthrough experiments conducted with simulated flue gas mixtures containing 3% NH_3 further confirm the impressive separation performance of DAL-NPs. Additionally, DAL-NPs exhibit notable structural stability and excellent reversibility over 10 cycles, indicating significant potential for NH_3 adsorption in industrial applications. This study demonstrates the effective use of waste industrial alkali lignin for the selective removal and capture of NH_3 from industrial flue gases. The reuse of waste material is of great importance, and this research provides a valuable contribution to this field.

■ ASSOCIATED CONTENT

Supporting Information

The Supporting Information is available free of charge at https://pubs.acs.org/doi/10.1021/acs.iecr.3c04306.

Characterization methods, ^{1}H NMR characterization, NH_3 adsorption procedure, breakthrough tests, breakthrough experiments apparatus, NH_3 adsorption apparatus, apparatus for the determination of NH_3 adsorption, breakthrough experiment apparatus, XPS curves for alkali lignin and DAL-NPs, TG curves of alkali lignin and DAL-NPs, isotope heat of DAL-NPs, FTIR spectra of fresh and 10 times regenerated DAL-NPs, and elemental analysis of the DAL-NPs adsorbent before and after desorption of NH_3 (PDF)

■ AUTHOR INFORMATION

Corresponding Authors

Zhang-Min Li − *National Engineering Research Center for Carbohydrate Synthesis, Key Laboratory of Fluorine and Silicon for Energy Materials and Chemistry of Ministry of Education, College of Chemistry and Chemical Engineering, Jiangxi Normal University, Nanchang 330022, China;* orcid.org/0000-0002-5001-1037; Email: zmli@jxnu.edu.cn

Duan-Jian Tao − *National Engineering Research Center for Carbohydrate Synthesis, Key Laboratory of Fluorine and*

https://doi.org/10.1021/acs.iecr.3c04306
Ind. Eng. Chem. Res. 2024, 63, 3282−3289

Silicon for Energy Materials and Chemistry of Ministry of Education, College of Chemistry and Chemical Engineering, Jiangxi Normal University, Nanchang 330022, China; orcid.org/0000-0002-8835-0341; Email: djtao@jxnu.edu.cn

Authors

Jian-Fei Li − *National Engineering Research Center for Carbohydrate Synthesis, Key Laboratory of Fluorine and Silicon for Energy Materials and Chemistry of Ministry of Education, College of Chemistry and Chemical Engineering, Jiangxi Normal University, Nanchang 330022, China*

Jian-Bo Xu − *National Engineering Research Center for Carbohydrate Synthesis, Key Laboratory of Fluorine and Silicon for Energy Materials and Chemistry of Ministry of Education, College of Chemistry and Chemical Engineering, Jiangxi Normal University, Nanchang 330022, China*

Cheng-Yong Guo − *National Engineering Research Center for Carbohydrate Synthesis, Key Laboratory of Fluorine and Silicon for Energy Materials and Chemistry of Ministry of Education, College of Chemistry and Chemical Engineering, Jiangxi Normal University, Nanchang 330022, China*

Guo-Wen Fang − *National Engineering Research Center for Carbohydrate Synthesis, Key Laboratory of Fluorine and Silicon for Energy Materials and Chemistry of Ministry of Education, College of Chemistry and Chemical Engineering, Jiangxi Normal University, Nanchang 330022, China*

Yan Zhou − *National Engineering Research Center for Carbohydrate Synthesis, Key Laboratory of Fluorine and Silicon for Energy Materials and Chemistry of Ministry of Education, College of Chemistry and Chemical Engineering, Jiangxi Normal University, Nanchang 330022, China;* orcid.org/0000-0003-0108-5061

Ming-Shuai Sun − *National Engineering Research Center for Carbohydrate Synthesis, Key Laboratory of Fluorine and Silicon for Energy Materials and Chemistry of Ministry of Education, College of Chemistry and Chemical Engineering, Jiangxi Normal University, Nanchang 330022, China;* orcid.org/0000-0002-5126-4159

Complete contact information is available at: https://pubs.acs.org/10.1021/acs.iecr.3c04306

Notes

The authors declare no competing financial interest.

■ ACKNOWLEDGMENTS

We thank the National Natural Science Foundations of China (nos. 22068013 and 22378178), the Natural Science Foundations of Jiangxi Province (no. 20232BAB203052), and the Key Lab of Fluorine and Silicon for Energy Materials and Chemistry of the Ministry of Education Jiangxi Normal University (no. KFSEMC-202209) for the financial support.

■ REFERENCES

(1) Yang, D.; Wu, X.; Qiu, X.; Chang, Y.; Lou, H. Polymerization Reactivity of Sulfomethylated Alkali Lignin Modified with Horseradish Peroxidase. *Bioresour. Technol.* **2014**, *155*, 418−421.

(2) Bernier, E.; Lavigne, C.; Robidoux, P. Y. Life Cycle Assessment of Kraft Lignin for Polymer Applications. *Int. J. Life Cycle Ass.* **2013**, *18*, 520−528.

(3) Zhou, M.; Kong, Q.; Pan, B.; Qiu, X.; Yang, D.; Lou, H. Evaluation of Treated Black Liquor Used as Dispersant of Concentrated Coal-Water Slurry. *Fuel* **2010**, *89*, 716−723.

(4) Gouveia, S.; Fernandez-Costas, C.; Sanroman, M. A.; Moldes, D. Enzymatic Polymerisation and Effect of Fractionation of Dissolved Lignin from Eucalyptus Globulus Kraft Liquor. *Bioresour. Technol.* **2012**, *121*, 131−138.

(5) Albadarin, A. B.; Al-Muhtaseb, A. H.; Al-laqtah, N. A.; Walker, G. M.; Allen, S. J.; Ahmad, M. N. M. Biosorption of Toxic Chromium from Aqueous Phase by Lignin: Mechanism, Effect of Other Metal Ions and Salts. *Chem. Eng. J.* **2011**, *169*, 20−30.

(6) Albadarin, A. B.; Collins, M. N.; Naushad, M.; Shirazian, S.; Walker, G.; Mangwandi, C. Activated Lignin-Chitosan Extruded Blends for Efficient Adsorption of Methylene Blue. *Chem. Eng. J.* **2017**, *307*, 264−272.

(7) Brdar, M.; Sciban, M.; Takaci, A.; Dosenovic, T. Comparison of Two and Three Parameters Adsorption Isotherm for Cr(VI) onto Kraft Lignin. *Chem. Eng. J.* **2012**, *183*, 108−111.

(8) Nair, V.; Panigrahy, A.; Vinu, R. Development of Novel Chitosan-Lignin Composites for Adsorption of Dyes and Metal Ions from Wastewater. *Chem. Eng. J.* **2014**, *254*, 491−502.

(9) Zhao, W.; Cui, Y.; Zhou, S.; Ye, J.; Sun, J.; Liu, X. Rapid Adsorption of Dyes from Aqueous Solutions by Modified Lignin Derived Superparamagnetic Composites. *J. Mol. Struct.* **2022**, *1261*, 132954.

(10) Hu, Z.; Liu, Y.; Lin, J.; Wu, H.; Liu, B.; Guo, W.; Lin, X.; Chen, L.; Qiu, X.; Qin, Y. Pyrene-Functionalized Alkali Lignin to Disperse Hydroxylated Boron Nitride Nanosheets in Cellulose Nanofibers for Thermal Management. *ACS Appl. Nano Mater.* **2023**, *6*, 200−211.

(11) Qin, Y.; Mo, W.; Yu, L.; Yang, D.; Qiu, X. A light-colored hydroxypropyl sulfonated alkali lignin for utilization as a dye dispersant. *Holzforschung* **2016**, *70* (2), 109−116.

(12) Qian, Y.; Deng, Y.; Qiu, X.; Li, H.; Yang, D. Formation of Uniform Colloidal Spheres from Lignin, A Renewable Resource Recovered from Pulping Spent Liquor. *Green Chem.* **2014**, *16*, 2156−2163.

(13) Nair, S. S.; Sharma, S.; Pu, Y.; Sun, Q.; Pan, S.; Zhu, J. Y.; Deng, Y.; Ragauskas, A. J. High Shear Homogenization of Lignin to Nanolignin and Thermal Stability of Nanolignin-Polyvinyl Alcohol Blends. *ChemSusChem* **2014**, *7*, 3513−3520.

(14) Erisman, J. W. How Ammonia Feeds and Pollutes the World. *Science* **2021**, *374*, 685−686.

(15) Vo, H. T.; Kim, J.; Kim, N. Y.; Lee, J.-K.; Joo, J. B. Effect of Pore Texture Property of Mesoporous Alumina on Adsorption Performance of Ammonia Gas. *J. Ind. Eng. Chem.* **2020**, *91*, 129−138.

(16) Deng, D.; Deng, X.; Li, K.; Fang, H. Protic Ionic Liquid Ethanolamine Thiocyanate with Multiple Sites for Highly Efficient NH_3 Uptake and NH_3/CO_2 Separation. *Sep. Purif. Technol.* **2021**, *276*, 119298.

(17) Binaeian, E.; Li, Y.; Yuan, D. Improving Ammonia Uptake Performance of Zirconium-Based Metal-Organic Frameworks Through Open Metal Site Insertion Strategy. *Chem. Eng. J.* **2021**, *421*, 129655.

(18) Hu, T.; Liu, F.; Dou, S.; Zhong, L.; Cheng, X.; Shao, Z.; Zheng, Y. Selective Adsorption of Trace Gaseous Ammonia from Air by A Sulfonic Acid-Modified Silica Xerogel: Preparation, Characterization and Performance. *Chem. Eng. J.* **2022**, *443*, 136357.

(19) Kim, D. W.; Kang, D. W.; Kang, M.; Choi, D. S.; Yun, H.; Kim, S. Y.; Lee, S. M.; Lee, J. H.; Hong, C. S. High Gravimetric and Volumetric Ammonia Capacities in Robust Metal-Organic Frameworks Prepared via Double Postsynthetic Modification. *J. Am. Chem. Soc.* **2022**, *144*, 9672−9683.

(20) Tian, J.; Liu, B. Y. Ammonia Capture with Ionic Liquid Systems: A Review. *Crit. Rev. Environ. Sci. Technol.* **2022**, *52*, 767−809.

(21) Wang, H.; Song, T.; Li, Z.; Qiu, J.; Zhao, Y.; Zhang, H.; Wang, J. Exceptional High and Reversible Ammonia Uptake by Two Dimension Few-layer BiI_3 Nanosheets. *ACS Appl. Mater. Interfaces* **2021**, *13*, 25918−25925.

(22) Luo, L.; Wu, Z.; Wu, Z.; Liu, Y.; Huang, X.; Ling, R.; Ye, L.; Luo, X.; Wang, C. Role of Structure in the Ammonia Uptake of

Porous Polyionic Liquids. *ACS Sustain. Chem. Eng.* **2022**, *10*, 4094−4104.
(23) Li, C. M.; Zhao, S. Y.; Li, M.; Yao, Z. L.; Li, Y.; Zhu, C. Q.; Xu, S. M.; Li, J. J.; Yu, J. The Effect of The Active Carbonyl Groups and Residual Acid on the Ammonia Adsorption Over the Acid-Modified Activated Carbon. *Front. Env. Sci.* **2023**, *11*, 976113.
(24) Cardenas, C.; Sigot, L.; Vallières, C.; Marsteau, S.; Marchal, M.; Latifi, A. M. Ammonia Capture by Adsorption on Doped and Undoped Activated Carbon: Isotherm and Breakthrough Curve Measurements. *Sep. Purif. Technol.* **2023**, *313*, 123454.
(25) Richard, A. J.; Chen, Z. J.; Islamoglu, T.; Farha, O. K.; El-Kaderi, H. M. Heteroatom-Doped Porous Carbons as Effective Adsorbers for Toxic Industrial Gasses. *ACS Appl. Mater. Interfaces* **2022**, *14*, 33173−33180.
(26) Zhu, F.; Wang, Z.; Huang, J.; Hu, W.; Xie, D.; Qiao, Y. Efficient Adsorption of Ammonia on Activated Carbon from Hydrochar of Pomelo Peel at Room Temperature: Role of Chemical Components in Feedstock. *J. Clean. Prod.* **2023**, *406*, 137076.
(27) Zong, K.; Li, K.; Zhou, Z.; Gong, L.; Deng, D. Highly Efficient and Reversible Adsorption of Ammonia by Incorporation of Deep Eutectic Solvents into Silica Gel and Al_2O_3. *New J. Chem.* **2022**, *46*, 15959−15966.
(28) Shen, C.; Wang, P.; Shen, L.; Yin, X.; Miao, Z. NH_3 Adsorption Performance of Silicon-Supported Metal Chlorides. *Ind. Eng. Chem. Res.* **2022**, *61*, 8616−8623.
(29) Shi, Y.; Wang, Z.; Li, Z.; Wang, H.; Xiong, D.; Qiu, J.; Tian, X.; Feng, G.; Wang, J. Anchoring LiCl in the Nanopores of Metal-Organic Frameworks for Ultra-High Uptake and Selective Separation of Ammonia. *Angew. Chem., Int. Ed.* **2022**, *61*, No. e202212032.
(30) Wang, Z.; Li, Z.; Zhang, X. G.; Xia, Q.; Wang, H.; Wang, C.; Wang, Y.; He, H.; Zhao, Y.; Wang, J. Tailoring Multiple Sites of Metal-Organic Frameworks for Highly Efficient and Reversible Ammonia Adsorption. *ACS Appl. Mater. Interfaces* **2021**, *13*, 56025−56034.
(31) Marsh, C.; Han, X.; Li, J.; Lu, Z.; Argent, S. P.; da Silva, I.; Cheng, Y.; Daemen, L. L.; Ramirez-Cuesta, A. J.; Thompson, S. P.; Blake, A. J.; Yang, S.; Schroder, M. Exceptional Packing Density of Ammonia in a Dual-Functionalized Metal-Organic Framework. *J. Am. Chem. Soc.* **2021**, *143*, 6586−6592.
(32) Khanpour Matikolaei, M.; Binaeian, E. Boosting Ammonia Uptake within Metal-Organic Frameworks by Anion Modulating Strategy. *ACS Appl. Mater. Interfaces* **2021**, *13*, 27159−27168.
(33) Tan, C.; Li, Z.; Sun, M.; Guan, H.; Zhou, Y.; Tao, D. Sulfonated Phenol-Formaldehyde Resins for Highly Efficient, Selective, and Reversible Adsorption of NH3. *Ind. Eng. Chem. Res.* **2023**, *62*, 1542−1549.
(34) Li, Z.; Long, J.; Zeng, Q.; Wu, Y.; Cao, M.; Liu, S.; Li, X. Production of Methyl *p*-Hydroxycinnamate by Selective Tailoring of Herbaceous Lignin Using Metal-Based Deep Eutectic Solvents (DES) as Catalyst. *Ind. Eng. Chem. Res.* **2020**, *59*, 17328−17337.
(35) Li, Z.; Cai, Z.; Zeng, Q.; Zhang, T.; France, L.; Song, C.; Zhang, Y.; He, H.; Jiang, L.; Long, J.; Li, X. Selective Catalytic Tailoring of the H Unit in Herbaceous Lignin for Methyl *p*-Hydroxycinnamate Production over Metal-Based Ionic Liquids. *Green Chem.* **2018**, *20*, 3743−3752.
(36) Harth, F. M.; Hočevar, B.; Kozmelj, T. R.; Jasiukaitytė-Grojzdek, E.; Blüm, J.; Fiedel, M.; Likozar, B.; Grilc, M. Selective Demethylation Reactions of Biomass-Derived Aromatic Ether Polymers for Bio-Based Lignin Chemicals. *Green Chem.* **2023**, *25*, 10117−10143.
(37) Zhao, W.; Wei, C.; Cui, Y.; Ye, J.; He, B.; Liu, X.; Sun, J. Efficient Demethylation of Lignin for Polyphenol Production Enabled by Low-Cost Bifunctional Protic Ionic Liquid under Mild and Halogen-Free Conditions. *Chem. Eng. J.* **2022**, *443*, 136486.
(38) Li, Z.; Sutandar, E.; Goihl, T.; Zhang, X.; Pan, X. Cleavage of Ethers and Demethylation of Lignin in Acidic Concentrated Lithium Bromide (ACLB) Solution. *Green Chem.* **2020**, *22*, 7989−8001.
(39) Chen, L.; Luo, S.; Huo, C.; Shi, Y.; Feng, J.; Zhu, J.; Xue, W.; Qiu, X. New Insight into Lignin Aggregation Guiding Efficient Synthesis and Functionalization of A Lignin Nanosphere with Excellent Performance. *Green Chem.* **2022**, *24*, 285−294.
(40) Zhang, H.; Ren, H.; Zhai, H. Analysis of Phenolation Potential of Spruce Kraft Lignin and Construction of Its Molecular Structure Model. *Ind. Crop. Prod.* **2021**, *167*, 113506.
(41) Sun, M.; Wang, X.; Ni, S.; Jiao, L.; Bian, H.; Dai, H. Structural Modification of Alkali Lignin into Higher Performance Energy Storage Materials: Demethylation and Cleavage of Aryl Ether Bonds. *Ind. Crop. Prod.* **2022**, *187*, 115441.
(42) Wang, H.; Eberhardt, T. L.; Wang, C.; Gao, S.; Pan, H. Demethylation of Alkali Lignin with Halogen Acids and Its Application to Phenolic Resins. *Polymers* **2019**, *11*, 1771.
(43) Han, Y.; Ma, Z.; Wang, X.; Sheng, Y.; Liu, Y. Demethylation of Ethanol Organosolv Lignin by Na_2SO_3 for Enhancing Antioxidant Performance. *Sustain. Chem. Pharm.* **2023**, *36*, 101312.
(44) Song, Y.; Wang, Z.; Yan, N.; Zhang, R.; Li, J. Demethylation of Wheat Straw Alkali Lignin for Application in Phenol Formaldehyde Adhesives. *Polymers* **2016**, *8*, 209.
(45) Zhu, S.; Li, Z.; Gong, W.; Gao, Z.; Guan, H.; Sun, M.; Zhou, Y.; Tao, D. Equimolar CO Capture by Cuprous-Based Quaternary Deep Eutectic Solvents. *Ind. Eng. Chem. Res.* **2023**, *62*, 2937−2943.
(46) Li, Z.; Zhu, S.; Mao, F.; Zhou, Y.; Zhu, W.; Tao, D. CTAB-Controlled Synthesis of Phenolic Resin-Based Nanofiber Aerogels for Highly Efficient and Reversible SO_2 Capture. *Chem. Eng. J.* **2022**, *431*, 133715.
(47) Li, Z.; Gong, W.; Li, J.; Zhu, S.; Tao, D.; Zhou, Y. Efficient and Selective Absorption of SO_2 by Low-Viscosity Matrine-Based Deep Eutectic Solvents. *J. Mol. Liq.* **2022**, *367*, 120521.
(48) Chen, Y.; Zhang, X.; Ma, K.; Chen, Z.; Wang, X.; Knapp, J.; Alayoglu, S.; Wang, F.; Xia, Q.; Li, Z.; Islamoglu, T.; Farha, O. K. Zirconium-Based Metal-Organic Framework with 9-Connected Nodes for Ammonia Capture. *ACS Appl. Nano Mater.* **2019**, *2*, 6098−6102.
(49) Lee, J. W.; Barin, G.; Peterson, G. W.; Xu, J.; Colwell, K. A.; Long, J. R. A Microporous Amic Acid Polymer for Enhanced Ammonia Capture. *ACS Appl. Mater. Interfaces* **2017**, *9*, 33504−33510.
(50) Jung, D.; Chen, Z.; Alayoglu, S.; Mian, M. R.; Goetjen, T. A.; Idrees, K. B.; Kirlikovali, K. O.; Islamoglu, T.; Farha, O. K. Postsynthetically Modified Polymers of Intrinsic Microporosity (PIMs) for Capturing Toxic Gases. *ACS Appl. Mater. Interfaces* **2021**, *13*, 10409−10415.
(51) Wu, G.; Xiao, J.; Yılmaz, M.; Zhang, T. C.; Yuan, S. Fusiform CuC_2O_4 Loaded Porous Biochar Derived from Phosphoric Acid-Activated Bagasse for Gaseous Ammonia Capture. *J. Environ. Chem. Eng.* **2023**, *11*, 109466.
(52) Zhang, J.; Ma, Y.; Wu, W.; Cai, Z.; Cao, Y.; Huang, K.; Jiang, L. Carboxylic functionalized mesoporous polymers for fast, highly efficient, selective and reversible adsorption of ammonia. *Chem. Eng. J.* **2022**, *448*, 137640.
(53) Zhang, J.; Ma, Y.; Wu, W.; Cai, Z.; Cao, Y.; Huang, K.; Jiang, L. Carboxylic Functionalized Mesoporous Polymers for Fast, Highly Efficient, Selective and Reversible Adsorption of Ammonia. *Chem. Eng. J.* **2022**, *448*, 137640.

https://doi.org/10.1021/acs.iecr.3c04306
Ind. Eng. Chem. Res. 2024, 63, 3282−3289